Nanoscale

RSC Publishing

PAPER

View Article Online
View Journal | View Issue

The effect of single wall carbon nanotube metallicity on genomic DNA-mediated chirality enrichment†

Cite this: *Nanoscale*, 2013, **5**, 4931

Steve S. Kim,[a] Colin L. Hisey,[ab] Zhifeng Kuang,[a] Donald A. Comfort,[b] Barry L. Farmer[a] and Rajesh R. Naik*[a]

Achieving highly enriched single wall carbon nanotubes (SWNTs) is one of the major hurdles today because their chirality-dependent properties must be uniform and predictable for use in nanoscale electronics. Due to the unique wrapping and groove-binding mechanism, DNA has been demonstrated as a highly specific SWNT dispersion and fractionation agent, with its enrichment capabilities depending on the DNA sequence and length as well as the nanotube properties. Salmon genomic DNA (SaDNA) offers an inexpensive and scalable alternative to synthetic DNA. In this study, SaDNA enrichment capabilities were tested on SWNT separation with varying degrees of metallicity that were formulated from mixtures of commercial metallic (*met*-) and semiconducting (*sem*-) abundant SWNTs. The results herein demonstrate that the degree of metallicity of the SWNT sample has a significant effect on the SaDNA enrichment capabilities, and this effect is modeled based on deconvolution of the near-infrared (NIR) absorption spectra and verified with photoluminescence emission (PLE) measurements. Using molecular dynamics and circular dichroism, the preferential SaDNA mediated separation of the (6, 5) *sem*-tube is shown to be largely influenced by the presence of *met*-SWNTs.

Received 25th January 2013
Accepted 3rd April 2013

DOI: 10.1039/c3nr00458a

www.rsc.org/nanoscale

Introduction

Due to their novel structure and properties, SWNTs have been heavily researched for potential use in a variety of applications.[1–5] In particular, their unique electrical properties[3] make them ideal candidates for nanoscale electronics. However, the use of commercially obtained SWNTs in such small scale electronics is limited by their inhomogeneity, since they are a mixture of chiralities and lengths.[6] Despite various efforts to control the synthesis and post-synthesis sorting techniques, the required chiral homogeneity of 99.999% remains to be a challenge. For most bulk SWNT post-synthesis separation methods, the SWNT aggregates must first be solubilized using a surfactant system or chemical functionalization. A chemically nondestructive, iteratively repeatable, economically feasible, widely compatible and scalable method is ideal,[7] and DNA has shown promise as a potential means of satisfying some or all of these criteria due to its nondestructive wrapping[8–13] and/or groove-binding[14] interactions. Following solubilization, the specific electrostatics of each DNA–SWNT hybrid, which is dependent on the DNA sequence and length as well as the diameter and electronic structure of the SWNT,[8,15] allow a variety of techniques to be employed in order to fractionate SWNTs according to their chirality, including density gradient ultracentrifugation[16] and ion exchange chromatography.[8,15] Recently SaDNA, an inexpensive byproduct of the fishing industry, has been shown to be a possible alternative to synthetic DNA to effectively solubilize[17] and fractionate[18] bulk samples of HiPco™ and SG65™ SWNTs. Based on NIR and PLE measurements, Kim *et al.*[18] demonstrated that SaDNA specifically enriches (6, 5) chirality SWNTs up to 86% in the supernatant fraction following sonication and ultracentrifugation with no further separation steps. In comparison, single stranded $d(GT)_{20}$ DNA-oligomer exhibited little to no chirality preference in this process. To date, the role of the specific DNA sequence and length have been the primary experimental variables due to their undeniably important role in selectivity dependence, with far less research focusing on the role of the electronic structure of the original bulk SWNT samples.

Probing the role of *met*-SWNTs ($n = m$, or $n - m = 3k$, where k is an integer) in the separation of *sem*-SWNTs ($n - m \neq 3k$), or *vice versa*, is a challenging issue for a single-source commercial grade nanotube due to the limits of current evaluation methods, such as UV-NIR absorbance, PLE, and resonance Raman scattering (RRS). For example, the UV-NIR absorbance spectra from typical *met*-SWNTs (E_{11}^{M} and/or E_{22}^{M}) overlap with those of *sem*-tubes (E_{22}^{S} and/or E_{33}^{S}) and their scattering, prohibiting qualitative and quantitative abundance evaluation for specific chirality nanotubes. In PLE, only *sem*-SWNTs produce

[a]*Materials and Manufacturing Directorate, Air Force Research Laboratory, Wright-Patterson AFB, Ohio 45433, USA. E-mail: Rajesh.Naik@wpafb.af.mil; Fax: +1 19372559157; Tel: +1 19372559717*

[b]*Chemical and Materials Engineering Department, University of Dayton, Dayton, Ohio, 45469, USA*

† Electronic supplementary information (ESI) available. See DOI: 10.1039/c3nr00458a

photoluminescence, while zero bandgap *met*-SWNTs do not. Typical RRS operates with a narrow resonance window for only certain nanotubes in resonance with its excitation laserline, thus demanding tuneable excitation laserlines to obtain spectra from a broad range of *met*-/*sem*-SWNTs. However, recent developments in carbon nanotube production enable one to commercially obtain higher semiconducting (SG65™, 15% *met*-SWNT) or metallic tube content SWNTs (CG200™, 39% *met*-SWNT) than stochastically produced 2 : 1 *sem*-:*met*-carbon nanotubes (HiPco™, 33.3% *met*-SWNT).[19] We show here that spectral measurements, including PLE and NIR absorption, on the quantitative mixtures of these samples can provide valuable insight into the role of *met*-SWNTs in the separation of *sem*-SWNTs. In this study, the preferential solubilization of a certain (n, m) SWNT is hypothesized to depend on the type of dispersant used,[18] and the degree of metallicity of the original SWNT sample. By combining the two types of SWNTs at different ratios and performing the dispersion and ultracentrifugation processes with SaDNA and sodium dodecyl sulfate (SDS), we demonstrate that *met*-SWNTs play an important role in the SaDNA-mediated (6, 5) SWNT enrichment by selectively interacting with the (6, 5) SWNTs based on NIR absorption studies. Moreover, we show that the (6, 5) chirality preference is reversed in the SaDNA solubilized CG200™ SWNTs, in contrast to the SG65™ sample based on extensive PLE measurements. Using circular dichroism (CD) and replica exchange molecular dynamics (REMD) we show that the inter-tube interaction is persistent in *sem*-(6, 5) and *met*-(11, 5) or -(7, 4) SWNTs with/without DNA, while the DNA significantly weakens the interaction energy between *sem*-(6, 5) and *sem*-(10, 3) or -(10, 6) tubes, and eventually exfoliates them.

Results and discussion

Sodium dodecyl sulfate (SDS) has been widely used as a dispersing agent for dispersing SWNTs into aqueous media. The E_{11}^S PLE emission contour plots from SDS dispersed SG65™ SWNTs (ESI, Fig. S1a and b†) and SDS dispersed CG200™ SWNTs (ESI, Fig. S1c and d†) in their redispersed precipitate and ultracentrifuged supernatant fractions show that in both samples of either *sem*- or *met*-abundant SWNTs, there are no apparent differences between the precipitate and supernatant fractions. These clearly indicate that SDS does not have chirality preference when dispersing the *sem*-rich SG65™ SWNTs and *met*-rich CG200™ SWNTs into aqueous media. Thus, SDS is first explored to verify that the proportionally reconstructed NIR spectra from homogeneous *sem*- and *met*-abundant commercial SWNTs are comparable to the spectra obtained from the dispersion made from their mixtures (Fig. 1 scheme). Six primary deconvoluted NIR absorption peaks from the supernatant fractions (see Materials and methods) are used to reconstruct predicted NIR spectra from the mixtures of commercial *sem*- and *met*-abundant SWNTs. Fig. 1a shows that the predicted NIR absorption spectrum of a SDS dispersed mixture of SG65™/CG200™ 1 : 3 (wt) SWNTs is nearly identical to the experimental data in Fig. 1b. These quantitative and qualitative similarities between predicted and experimental NIR

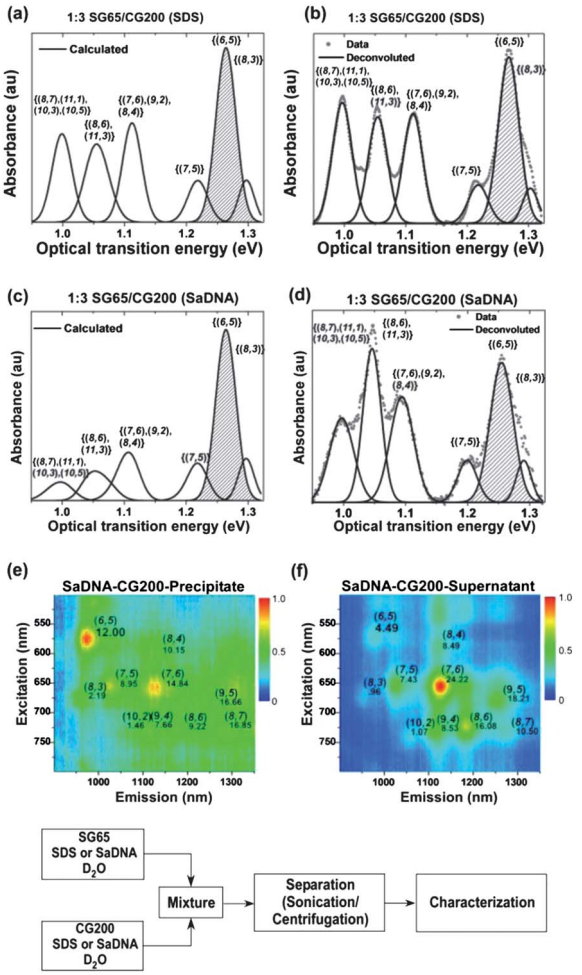

Fig. 1 Calculated (a) and actual (b) E_{11}^S NIR absorption profiles of a SDS dispersed 1 : 3 SG65™/CG200™ SWNT mixture in the ultracentrifuged supernatant fractions. Calculated (c) and actual (d) E_{11}^S NIR absorption profiles of a 1 : 3 SG65™/CG200™ SWNT mixture dispersed with SaDNA, ultracentrifuged supernatant fractions. Groups of the characteristic NIR E_{11}^S peaks are deconvoluted and assigned with respect to their possible chiralities and indicated as groups in brackets "{ }".[20,21] (6, 5) SWNT peaks are shaded for visualization. E_{11}^S PLE emission contour plots (e and f) from SaDNA dispersed CG200™ SWNTs in the redispersed precipitate and ultracentrifuged supernatant fractions, respectively. PLE peaks are normalized with respect to the maximum intensity SWNT PLE peak for the visualization of relative chirality fractions. Scheme shows the process of mixing, separation, and characterization of SG65™/CG200™ SWNTs with SDS or SaDNA.

spectra from the above SDS-dispersed SWNT mixture validate the use of NIR peak reconstruction of commercial nanotubes with various metallicities for studying their interactions, specifically the effects of *met*-SWNTs in the separation of *sem*-SWNTs.

Fig. 1c shows the SG65™/CG200™ 1 : 3 (wt) mixture peaks reconstructed from the peak fitting model based on 100% CG200™ and 100% SG65™ SaDNA aqueous SWNT dispersion. The six peaks, when compared to the experimental data (Fig. 1d), show a significant decrease of the 1.27 eV peak, indicating the exclusion of (6, 5) tubes in the presence of *met*-abundant tubes. Moreover, PLE measurements of the pure CG200™ *met*-SWNT fraction (Fig. 1e and f) demonstrate a reversal in the previously demonstrated (6, 5) chirality

enrichment trend,[18] when samples containing mostly *sem*-SWNTs were used with SaDNA as a dispersant. In the previous study, we showed the enrichment of (6, 5) SWNTs from a SG65™ (mean diameter, $\overline{d_t} = 0.81$ nm, 15% *met*-) sample of ~86% in the supernatant fraction (see ESI Fig. S2a†) and similar increases in (6, 5) SWNTs for a HiPco™ ($\overline{d_t} = 1.05$ nm, 33.3% *met*-) sample, indicating that the preferential SaDNA–(6, 5) SWNT interaction is not dependent on the diameter distribution of the original nanotube sample. However, for CG200™ (highly *met*-, $\overline{d_t} = 1.01$ nm, 39% *met*-) SWNTs, the concentration of (6, 5) chirality SWNTs in the redispersed-precipitate (Fig. 1e) is >2× that of the ultracentrifuged supernatant (Fig. 1f), demonstrating (6, 5) exclusion rather than enrichment with SaDNA as the dispersing agent. The corresponding E_{11}^S PLE emission contour plots from SaDNA dispersed 1 : 0, 3 : 1, 1 : 3, and 0 : 1 SG65™/CG200™ SWNT mixtures in the ultracentrifuged supernatant fraction showing corresponding (6, 5) exclusion are shown in Fig. S2a–d.† (6, 5) Exclusion in the supernatant found for the SG65™/CG200™ 3 : 1 mixture (see ESI Fig. S2b and S3†) indicates that at even low concentrations, *met*-SWNTs can impact SaDNA's fractionation ability. Collectively, the data indicate that the starting fraction of metallic nanotubes has a strong effect on the (6, 5) enrichment capabilities of SaDNA. Thus, both the type of dispersion medium used and the degree of metallicity of the original SWNT mixture must be considered when attempting to enrich bulk SWNT samples, as both factors can greatly affect the final chirality concentrations in the supernatant fractions.

Further studies were carried out to determine whether the *met*-tube induced (6, 5) exclusion for the SaDNA–SWNT dispersion is a spectroscopic artifact by simply mixing the post-processed *sem*- and *met*-SWNT supernatant fractions without following the ultrasonication process (Fig. S4† scheme). The NIR absorption profiles obtained from post-processed 1 : 3 (Fig. S4a†) and 3 : 1 (Fig. S4b†) SG65™/CG200™ SaDNA dispersion mixtures are closer to their respective calculated spectra in Fig. 1c and S3a† when compared to their counterparts in Fig. 1d and S3b,† respectively. These results indicate that there is no significant spontaneous diffusion-driven (6, 5) exclusion/enrichment due to the *met*-(6, 5) tube–tube interaction in the post-process supernatants as compared to the mixing and separation process shown in Fig. 1.

Circular dichroism has been used to determine the helicity of DNA by monitoring the intensity changes from the negative and positive peaks at 290–260 nm (P^+) and 260–230 nm (P^-), respectively.[22] The relative increase in P^+ as compared to P^- indicates that the DNA restructures to A-form from its more dominant B-form. Along with several CD studies that observed SWNT-induced structural change of DNA helicity,[23,24] we previously showed the SaDNA transitions from its native B-form to a near-A-form in the presence of HiPco™ SWNTs.[18] Interestingly, the CD spectra (Fig. 2a) acquired from SaDNA dispersed SG65™ show higher increase in the P^+/P^- ratio when compared with SaDNA dispersed CG200™ SWNTs. From this P^+/P^- trend, we speculate that the SaDNA forms a compact A-like DNA form with SG65™, more specifically with (6, 5) SWNTs, than with CG200™. The SaDNA–tube interaction weakened by the

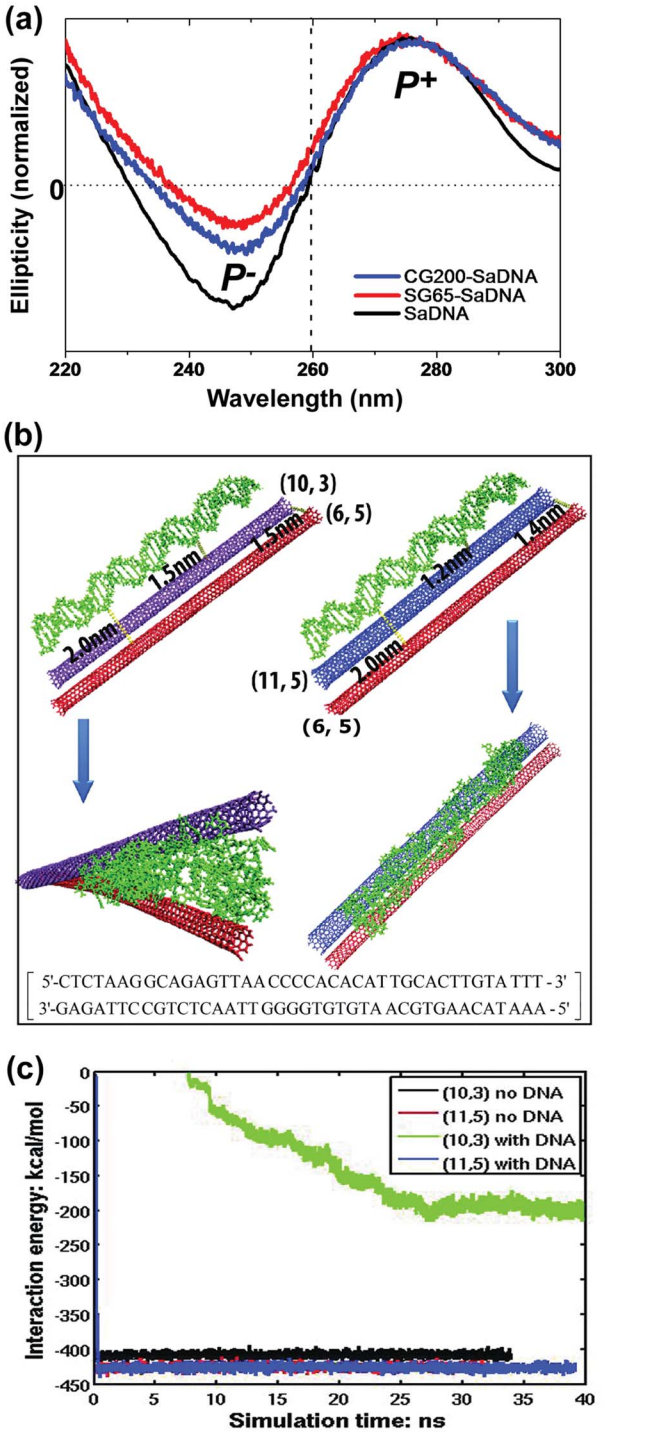

Fig. 2 (a) Normalized CD spectra from SaDNA and SaDNA dispersed SG65™ and CG200™ SWNTs. The SaDNA CD spectrum shows complete B-form. The negative and positive peaks at 290–260 nm and 260–230 nm are noted as P^+ and P^-, respectively. Replica exchange molecular dynamics simulation showing the tube–tube interaction of SWNTs with/without SaDNA; (b) initial and end-point (after 40 ns simulation) configurations of the (6, 5) SWNT in the presence of DNA/(10, 3) SWNT and DNA/(11, 5) SWNT; (c) the time evolution of the interaction energy (kcal mol^{-1}) of (6, 5) with a semiconducting tube (10, 3) or a metallic tube (11, 5) in the presence or absence of SaDNA. The model SaDNA sequence is shown in (b).

abundant *met*-SWNTs is believed to be due to the lesser degree of B to A transition in the presence of CG200™ SWNTs. The observed higher degree of B- to A-form transition in SG65™–SaDNA than CG200™–SaDNA agrees well with the structural changes obtained from the following MD simulation, where the A-like helical structure is more dominant when the (6, 5)-tube is mixed with a *sem*-SWNT rather than with a *met*-SWNT. Classical all-atom MD simulation is a useful tool to understand why SaDNA has preferential binding affinity to (6, 5) tubes rather than other *sem*-SWNTs, such as (10, 3) tubes present in HiPco™ and SG65™ samples.[18] We have further exploited replica exchange molecular dynamics (REMD) to monitor the time evolution of the van der Waals interaction between (6, 5):(10, 3) and (6, 5):(11, 5) tubes in the presence of SaDNA in a vacuum. The *met*-(11, 5) tube was chosen since the (11, 5) SWNT is persistently observed as a 218 cm^{-1} peak at 1.96 eV RRS spectra[25] from the SaDNA dispersed HiPco™ SWNT.[18]

The length of SWNTs is set to be 16 nm leaving a 1.2 nm margin at each end to avoid the edge effect when the 13.6 nm long model double strand SaDNA (40 base pairs) is placed above the SWNTs. The terminal carbon atoms at both ends of a SWNT are terminated with hydrogen atoms. SWNTs are modelled as flexible molecules with 3D translational and rotational degree of freedom. The AMBER 99SB force field is used in all simulations. Fig. 2b shows the initial and final configurations of parallel-positioned SWNTs and SaDNA in a perspective view with their mutual distances. In order to avoid biased initial mutual interactions, the initial pair-wise distances between components are set to be slightly larger than the cut-off distance, 1.2 nm. Using a Langevin thermostat, the system temperature is gradually increased from 0 K to 300 K while keeping the constituents in random thermal motion. The convergence to a lower energy configuration is expedited by allowing a high temperature conformational search process to provide feedback to the low temperature process. REMD simulations consisting of 8 replicas with exponentially spaced temperature from 300 K to 600 K are performed using NAMD2.9 for 40 ns. After the 40 ns simulations, the trajectories corresponding to temperature 300 K are analysed. The end-point configuration at 300 K shows that SaDNA preferentially wraps the (6, 5) tube preventing its aggregation with the (10, 3) tube, which is in agreement with our previous observation.[18] Meanwhile, SaDNA does not interact well with the (6, 5) tube in the presence of the *met*-(11, 5) tube, leaving the (6, 5) and (11, 5) as an aggregated bundle. The detailed tube–tube interaction energy in the absence or presence of SaDNA is shown in Fig. 2c. The adsorption energy (the absolute value of van der Waals interaction energy) between (6, 5) and SaDNA (392.4 ± 6.3 kcal mol^{-1})[18] is comparable to the (6, 5):(10, 3) adsorption energy of 408 ± 4 kcal mol^{-1}. As a result, the SaDNA is able to compete with the (6, 5):(10, 3) tube–tube bundling, significantly decreasing the (6, 5):(10, 3) adsorption energy to 200 ± 6 kcal mol^{-1}. However, the (6, 5) and SaDNA interaction energy is lower than the adsorption energy between (6, 5) and (11, 5) tubes (431 ± 4 kcal mol^{-1}). These MD-based interaction energy profiles of the (6, 5) tube–SaDNA system with a *sem*-(10, 3) and a *met*-(11, 5) support our experiment that has shown the interfering role of *met*-tubes in the (6, 5) SWNT enrichment using SaDNA. We further investigated whether the tube diameter affects the interaction energy of (6, 5):*met*-SWNTs and (6, 5):*sem*-SWNTs using MD simulation (Table 1). As expected, the adsorption energy increases with increasing diameters of the tubes in contact with the (6, 5) SWNTs in the absence of DNA. However, in the presence of DNA, the *sem–sem* tube adsorption energy significantly decreases from 408 to 200 kcal mol^{-1}, and from 429 to 360 kcal mol^{-1} for (6, 5):(10, 3) and (6, 5):(10, 6) pairs, respectively. In comparison, the *sem–met* tube interaction adsorption energy remains unchanged for both small diameter (7, 4) and large diameter (11, 5) tubes. This implies that metallicity plays the dominant role in the genomic DNA-mediated (6, 5) tube enrichment rather than the diameter of the SWNTs. Detailed studies on the diameter and chirality distribution effects on tube–tube interactions in the presence of SaDNA are underway in our laboratory.

Table 1 The adsorption energy (kcal mol^{-1}) between (6, 5) and other types of tubes in the presence or absence of SaDNA

	(10, 3)	(10, 6)	(7, 4)	(11, 5)
Diameter (nm)	0.92	1.10	0.76	1.11
Energy (kcal mol^{-1})	408 ± 4	429 ± 4	389 ± 3	431 ± 4
Energy (kcal mol^{-1}) + SaDNA	200 ± 6	360 ± 4	388 ± 3	428 ± 4

Conclusions

By using NIR absorption measurements on the *sem*- or *met*-abundant commercial SWNT samples and their mixtures as the starting material in the dispersion process, we developed a simple and useful method for comparing SWNT mixture chirality enrichments. This peak-fitting based spectral reconstruction method can be an effective tool to evaluate the SWNT chirality/metallicity effect on the separation processes. We have shown that the degree of metallicity of the starting SWNT sample plays an important role in the SaDNA-mediated enrichment of (6, 5) tubes. Molecular dynamics simulation shows that the (6, 5) tube disaggregates from the *sem*-tubes in the presence of SaDNA, while the interaction with *met*-tubes fails to result in dispersion in the presence of saDNA. It must be emphasized that the degree of metallicity in an original SWNT mixture must be taken into account for dispersion-based chirality-enrichment procedures for SWNTs, such as ion exchange chromatography,[9] dielectrophoresis,[26] and ultracentrifugation.[27] We are in the process of developing the effective integration of the pre-enrichment *met*-SWNT separation techniques, such as dielectrophoresis, to the current DNA-based process for achieving consistently high chiral homogeneity from commercial SWNTs.

Materials and methods

The >8 MDa (million daltons) SaDNA was prepared following the process appears elsewhere.[28] The typical enrichment process involved sonication of SWNTs with SaDNA or sodium

dodecyl sulfate (SDS) surfactant in D_2O, followed by a series of centrifugations. CG200™ SWNTs (SouthWest NanoTechnologies, Norman, OK) were used for the primarily *met*-SWNT source, and SG65™ SWNTs (SouthWest NanoTechnologies) were used for the primarily *sem*-SWNT source. The initial dispersion of the different SWNT samples was achieved by combining either CG200™ or SG65™ SWNTs at a concentration of 0.5 mg mL^{-1} in D_2O with 1 mg DNA per mL D_2O. These mixtures were sonicated using a 750 W tip-horn ultrasonicator (SONICS Vibra Cell) at 35% amplitude for 20 minutes. During all sonication steps, the samples were cooled *via* submersion in an ice bath to prevent vapor loss. Following the initial sonication, the two dispersed samples were combined at ratios of 0 : 1, 1 : 3, 3 : 1 and 1 : 0 SG65™/CG200™ by volume (5 mL total for each ratio). By creating these mixtures from the same original two solutions after the initial sonication, we minimized the variance in the mass concentration of SWNTs between samples, which proved difficult to control if the SWNTs are combined prior to sonication. These four mixtures were diluted with 4 mL D_2O each and then underwent further sonication at the same amplitude for an additional 35 min to ensure the maximum degree of dispersion. Following sonication, each mixture underwent a "light" centrifugation at 14 000 $\times$ *g* for 90 minutes (Eppendorf 5804) in order to separate the solubilized SWNTs from the non-dispersed SWNTs. The supernatants for each mixture from the "light" centrifugation were carefully removed and then centrifuged at 610 000 $\times$ *g* for 60 minutes (Sorvall RCM120). Following ultracentrifugation, the supernatants were meticulously removed so as to not disturb the precipitate, and the remaining precipitates were combined for subsequent characterization. Control SWNT enrichment experiments were performed using 1 wt% SDS dispersed solutions instead of SaDNA. SDS was chosen because it lacks chiral preference for SWNTs and is inexpensive compared to the $d(GT)_{20}$ DNA-oligomer. Comparable sonication procedures, dilutions and centrifugations were performed to ensure a consistent means for comparison. pH in both SDS- and SaDNA-dispersed SWNTs was measured to be neutral. Control post-process mixtures were created using the ultracentrifuged supernatants from the original CG200™ and SG65™ samples. 0 : 1, 1 : 3, 3 : 1, and 1 : 0 SG65™/CG200™ mixtures of the supernatants were simply shaken by hand, aged over a period of one week, and their PLE and NIR spectra were measured.

PLE emission spectra were acquired using a spectrofluorometer (Horiba-Jobin-Yvon Nanolog™) to analyze *sem*-SWNT chirality concentrations in the ultracentrifuged supernatant and precipitate fractions. Relative fractions of particular (*n*,*m*) chiralities in the PLE spectra were determined by comparing the maximum intensity ($I^{PL}_{(n,m)}$) at each known excitation and emission wavelength for corresponding E^S_{11} transitions between valence and conduction bands according to their distinct van Hove singularities (vHs). These PLE measurements were weighted by their intensity values based on their induced photon-absorption, relaxation rate at E^S_{22} and spontaneous photon-emission matrix elements[29] ($q_{(n,m)}$). The particular (*n*,*m*) relative fractions of the measured *sem*-SWNTs were defined as the corrected intensity divided by the sum of all the corrected intensities in the measured E^S_{11} range,[25] according to:

$$RF^{PL}_{SaDNA} = \frac{I^{PL}_{(n,m)}/q_{(n,m)}}{\sum I^{PL}_{(n,m)}/q_{(n,m)}}$$

NIR spectra were obtained using a spectrophotometer (PerkinElmer Lambda 900). Deconvoluted NIR absorption profiles were generated using the peak fitting module in Origin™ software (Origin Lab Co., MA). Six primary Gaussian curves for the SWNTs used in this experiment were selected within the 900–1305 nm range as a means of analysis and model development. The Gaussian curves were fit with fixed baseline parameters, confidence of 0.95 and tolerance of 0.05. For the model, the six characteristic NIR absorption peaks (i) of the CG200™ and SG65™ ultracentrifuged supernatant fractions for SaDNA and SDS were weighed according to their % volume (ν) in the combined mixtures, according to the equation:

$$[Abs_{mix,i}(x)] = \nu_{CG200}[Abs_{CG200,i}(x)] + \nu_{SG65}[Abs_{SG65,i}(x)],$$
$$\text{for } i = 1, 2, \ldots 6,\ 0.95 < x < 1.35 \text{ eV}.$$

Acknowledgements

Funding for this research was provided by Air Force Office of Scientific Research (AFOSR), Air Force Base Research Laboratory (AFRL/RX), and the University of Dayton Minority Leaders Program. The authors thank Dr Grote at AFRL/RX and Prof. Ogata at Chitose Institute of Science and Technology in Japan for kindly providing materials; Ms Issa and Prof. Browning at the University of Dayton for their technical support and helpful discussions.

Notes and references

1 P. M. Ajayan and O. Z. Zhou, *Top. Appl. Phys.*, 2001, **80**, 391–425.
2 M. Terrones, *Annu. Rev. Mater. Res.*, 2003, **33**, 419–501.
3 P. R. Bandaru, *J. Nanosci. Nanotechnol.*, 2007, **7**, 1239–1267.
4 M. Endo, M. Strano and P. Ajayan, *Topics in Applied Physics,* Springer Berlin/Heidelberg, 2008, vol. 111, pp. 13–61.
5 J. F. Rusling, S. N. Kim and F. Papadimitrakopoulos, *Adv. Mater.*, 2007, **19**, 3214–3228.
6 D. Chattopadhyay, I. Galeska and F. Papadimitrakopoulos, *J. Am. Chem. Soc.*, 2003, **125**, 3370–3375.
7 M. C. Hersam, *Nat. Nanotechnol.*, 2008, **3**, 387–394.
8 M. Zheng, A. Jagota, M. S. Strano, A. P. Santos, P. Barone, S. G. Chou, B. A. Diner, M. S. Dresselhaus, R. S. Mclean, G. B. Onoa, G. G. Samsonidze, E. D. Semke, M. Usrey and D. J. Walls, *Science*, 2003, **302**, 1545–1548.
9 M. Zheng, A. Jagota, E. D. Semke, B. A. Diner, R. S. McLean, S. R. Lustig, R. E. Richardson and N. G. Tassi, *Nat. Mater.*, 2003, **2**, 338–342.
10 B. Gigliotti, B. Sakizzie, D. S. Bethune, R. M. Shelby and J. N. Cha, *Nano Lett.*, 2006, **6**, 159–164.

11 Q.-H. Yang, N. Gale, C. J. Oton, F. Li, A. Vaughan, R. Saito, I. S. Nandhakumar, Z.-Y. Tang, H.-M. Cheng, T. Brown and W. H. Loh, *Nanotechnology*, 2007, **18**, 405706.
12 S. Toita, D. Kang, K. Kobayashi, H. Kawamoto, K. Kojima and M. Tachibana, *Diamond Relat. Mater.*, 2008, **17**, 1389–1393.
13 Q.-H. Yang, Q. Wang, N. Gale, C. J. Oton, L. Cui, I. S. Nandhakumar, Z. Zhu, Z. Tang, T. Brown and W. H. Loh, *Nanotechnology*, 2009, **20**, 195603.
14 G. Lu, P. Maragakis and E. Kaxiras, *Nano Lett.*, 2005, **5**, 897–900.
15 X. Tu, S. Manohar, A. Jagota and M. Zheng, *Nature*, 2009, **460**, 250–253.
16 M. S. Arnold, S. I. Stupp and M. C. Hersam, *Nano Lett.*, 2005, **5**, 713–718.
17 Y. Asada, H. Dohi, S. Kuwahara, T. Sugai, R. Kitatura and H. Shionohara, *Nano*, 2007, **02**, 295–299.
18 S. N. Kim, Z. Kuang, J. G. Grote, B. L. Farmer and R. R. Naik, *Nano Lett.*, 2008, **8**, 4415–4420.
19 S. Cambrao, W. Wenseleers, E. Goovaerts and D. E. Resasco, *ACS Nano*, 2012**4**, 6717–6724.
20 S. M. Bachilo, M. S. Strano, C. Kittrell, R. H. Hauge, R. E. Smalley and R. B. Weisman, *Science*, 2002, **298**, 2361–2366.
21 Z. Luo, L. D. Pfefferle, G. L. Haller and F. Papadimitrakopoulos, *J. Am. Chem. Soc.*, 2006, **128**, 15511–15516.
22 W. A. Baase and W. C. Johnson, Jr, *Nucleic Acids Res.*, 1979, **6**, 797–814.
23 D. A. Heller, E. S. Jeng, T.-K. Yeung, B. M. Martinez, A. E. Moll, J. B. Gastala and M. S. Strano, *Science*, 2006, **311**, 508–511.
24 X. Li, Y. Peng and X. Qu, *Nucleic Acids Res.*, 2006, **34**, 3670–3676.
25 E. Menna, F. Della Negra, M. Dalla Fontana and M. Meneghetti, *Phys. Rev. B: Condens. Matter*, 2003, **68**, 193412.
26 H. Peng, N. T. Alvarez, C. Kittrell, R. H. Hauge and H. K. Schmidt, *J. Am. Chem. Soc.*, 2006, **128**, 8396–8397.
27 E. H. Hároz, W. D. Rice, B. Y. Lu, S. Ghosh, R. H. Hauge, R. B. Weisman, S. K. Doorn and J. Kono, *ACS Nano*, 2012**4**, 1955–1962.
28 L. Wang, J. Yoshida, N. Ogata, S. Sasaki and T. Kajiyama, *Chem. Mater.*, 2001, **13**, 1273–1281.
29 Y. Oyama, R. Saito, K. Sato, J. Jiang, G. G. Samsonidze, A. Gruneis, Y. Miyauchi, S. Maruyama, A. Jorio, G. Dresselhaus and M. S. Dresselhaus, *Carbon*, 2006, **44**, 873–879.

